The potential of satellite gravity and gravity gradiometry in deciphering structural setting of the Himalayan Collision Zone

V. M. Tiwari*, B. Singh, K. Arora and S. Kumar

National Geophysical Research Institute (CSIR), Hyderabad 500 606, India

During the last decade, three dedicated satellite gravity missions (CHAMP, GRACE and GOCE) have greatly improved the knowledge of the static and dynamic gravity field of the Earth. Bouguer gravity anomalies (BGA) derived from global gravity models (e.g. EGM2008), which consist of GRACE satellite observations and terrestrial gravity data, are analysed to demonstrate through selected applications, their potential use in studying large scale geological features of the Himalaya, where little or no terrestrial data are available. A constrained 3D lithospheric density model over a part of the Eastern Himalayan region is constructed from modelling of BGA and utilized to calculate forward responses of selected gravity gradient (GG) tensors, highlighting certain aspects of the structural features of the Himalayan Collision Zone (HCZ). In addition, GG are also computed directly from BGA by Fourier transformation to study the additional information content they may provide. This exercise may demonstrate the extra advantages of modelling gravity gradiometry measurements, which is of high contemporary relevance in view of the fact that satellite gravity gradient data from the ongoing GOCE mission will be available shortly. We find that structural features like Main Boundary Thrust, Main Central Thrust are sharply reflected in GG and combined interpretation of BGA and GG can better resolve the locations and possibly the depth extent of the density anomalies. BGA is also utilized to constrain crustal thickness variation and used along with topography to estimate variation of effective elastic thickness across the Eastern Himalayan region.

Keywords: Gravity and gradiometry, GRACE, GOCE, Himalaya, isostasy.

Introduction

THE collision of the Indian plate with the Eurasian plate during the Eocene has created the spectacular features of Himalaya and Tibet[1]. In the continued journey of the Indian plate towards north, rocks are crumpled, folded, faulted and thrusted upward, forming several large structural and tectonic features extending over thousands of kilometres, preserving imprints of the collision processes. One of the highest mountains in the world, Himalaya is formed due to this collision. The excess mass of the Himalayan topography is compensated at depth as thickened crust and produces large negative Bouguer gravity anomalies[2–6]. Thus the Himalayan Collision Zone (HCZ) comprises thrust faults, subducted lithosphere, thickened crust below mountain belts, and suture zones, which are reflected in the patterns of gravity anomalies. Study of satellite-derived gravity signals for interpretation of regional structure is well accepted[7]. Here we study whether additional use of gravity gradients (GGs) can aid the interpretation of tectonic features. Although GG measurements using the torsion balance were in use as early as 1915, mainly for exploration purposes, their applications in lithospheric studies are a relatively new experience[8]. A core component of the present work is to process global gravity data and calculate the gradient components from them as well from a constrained 3D density and structural model of the lithosphere in the frontier tectonic setting of Eastern Himalaya with the objective to better understand the gradient signatures of lithospheric structures. Preliminary results provide characteristic gradient signatures of major structural features and will be of great importance, when measured GG data from the Gravity field and steady-state Ocean Circulation Explorer (GOCE) satellite mission will eventually be available. In this study we have also computed lithospheric rigidity in frontier regions where little or no surface data are available.

Gravity and gradiometry measurements from satellites

The history of measurements of the variations of the global gravity field from space, using satellite technology is more than three decades old, dating back to the JPL SEASAT mission in 1978 (based on space-borne SAR and radar altimeter) and GEOSAT mission in 1985 (radar altimeter, with exact repeat orbits). ERS-1 (1991), ERS-2 (1995) and ENVISAT-1 (2002–2007) followed, equipped with Satellite Laser Ranging (SLR) (see ref. 9 and references therein), which was used to calibrate the radar

*For correspondence. (e-mail: vmtiwari@ngri.res.in)

altimeter. The radar altimeter data was used to determine ocean surface heights, which in turn, is used to monitor global ocean circulation, regional ocean current systems, and study of the marine gravity field.

In the last decade, a series of three dedicated gravity field missions have been flown with new technology. CHAllenging Minisatellite Payload (CHAMP; in orbit from July 2000 to September 2010) is the first mission that combined Satellite-to-Satellite Tracking with the GPS constellation (SST-*hl*) along with 3D accelerometry[10]. The Gravity Recovery And Climate Experiment (GRACE) mission (started in March 2002)[11–13] employs the concept of satellite-to-satellite tracking between two low orbiters (SST-*ll*) in the same orbit at a distance of about 200 km. The nongravitational forces are measured accurately using the 3D accelerometers onboard the twin satellites. The satellite tracking data, which are influenced by the minute variations in the Earth's gravity field, have been able to generate long wavelength gravity anomaly maps of the entire Earth. Recently, the GOCE has been launched in March 2009 on the principle of satellite gradiometry[14–16], whereby the natural signal attenuation at satellite altitude is counteracted by measurements of the differential acceleration. The total gravity field calculated from GG tensor data is expected to yield a geoid error below the cm level and a gravity anomaly error just below 0.08 mGal for the static field to the degree 200 (100 km resolution). Thus we have progressively higher resolution gravity fields from satellite measurements.

While a conventional gravity survey records a single component of the three-component gravitational force F, usually in the vertical plane; Full Tensor Gravity Gradiometry (FTG, as in GOCE) measures the derivative of all three components in all three directions. Since div $F = 0$ and curl $F = 0$, only five of the nine components are independent. The theoretical foundations of gravity gradiometry are given by Rummel[17]. It is possible to compute the gradients from the total field and vice versa using mathematical relationships. Thus in theory no measurement system holds any advantage over the other. However, in practice, adequate accuracy and resolution is not achieved by each kind of measurement in each situation. Geoid measurements are most suitable for the longest wavelengths and gradient measurements for the shortest wavelengths.

Gravity and gradient maps of the Himalaya

Several new global gravity models are now available such as EIGENGL04C (ref. 18) and EGM2008 (ref. 19), which include data from GRACE satellite mission for long wavelengths (low degree and order of spherical harmonics) and terrestrial data for short wavelengths. Gravity field of the EIGENGL04C model is computed for spherical harmonics of degree and order 360. It combines GRACE data for spherical harmonic coefficients up to degree and order 70, amalgamation of satellite and terrestrial data at intermediate wavelength and terrestrial data at short wavelength (higher spherical harmonics of 115–360). The EGM2008 gravity model is complete to the spherical harmonics of degree and order 2159 and also combines primarily the satellite and surface measurements[19]. The EGM2008 model is computed for higher spherical harmonics and thus its spatial resolution is comparatively more than the EIGENGL04C model. However, in the regions like Himalaya, where very few surface measurements are available, both the models are likely to be the same. We compared both the models over Indian region as well as a part of Sikkim Himalaya and find that EGM2008 contains better representation of short wavelengths, which might be because EGM2008 includes more terrestrial data to compute the higher spherical harmonics. With this consideration, we preferred to use the EGM2008 model and computed free-air gravity anomaly on the surface from spherical harmonics of EGM2008. Correction for elevation effects in the gravity data is a meticulous effort for Himalayan terrain. We have used GTOPO30 digital terrain model[20] for this purpose. Bouguer slab correction is applied for density 2670 kg/m^3. The terrain effects are computed over a large region extending 200 km beyond the HCZ. Terrain correction is as large as 70–80 mGal at some locations. To bring terrain effects to an identical wavelength, gravity anomaly and effects are filtered using low pass digital filter before corrections are applied to gravity data. Filtering is done in two steps: one for foreland (30 km wavelength), where short wavelength Bouguer gravity anomalies (BGA) match well with surface Bouguer anomalies and then for grids over Himalaya and Tibet (75 km wavelength). Then both grids are compared and amalgamated. The complete Bouguer anomalies derived from this global gravity model are validated vis-à-vis complete Bouguer anomalies computed along a set of profiles (from Sikkim and Nepal Himalaya) of measured data and are found to be satisfactory for the requirements of this study (Figure 1). Assuming that this comparison would be valid over the region around Sikkim and Nepal, Bouguer anomaly map of the entire central HCZ is computed and presented in Figure 2. Broadly, the Bouguer anomaly is negative over the Himalayan Mountain and Tibet plateau region, suggesting compensation of topography at depth. However, the lowest value is not under the highest mountain signifying that lithospheric stresses support the Himalayan topography to varying extents.

Although the gradient tensor measurements from the GOCE mission are awaited, we have computed selected GG tensors from BGA using the Fast Fourier Transform method[21]. Figure 3 shows the nine tensors of gravity gradiometry and their directions. Computed GG tensors are sensitive to the quality of Bouguer anomaly data used, thus we have compared BGA with surface data (Figure 1)

to affirm that computed GG tensors are not artefacts. Furthermore, computed GG is evaluated with response of the subsurface structure in the following section. Although computed GG tensors cannot replace the actual gradient tensor measurement, FFT derived gradients closely approximate the true gradients[8] and provides a basis to study the nature of gradients with respect to the configuration of density sources. The different components of GG tensors have specific properties. The G_{zz} component can provide an estimate of the location and the shape of the causative sources. G_{zy} and G_{yy} offer to locate those structures trending in E–W direction. Maps of three tensor components, G_{zy}, G_{yy} and G_{zx}, are plotted in Figure 4. Interestingly, G_{zy} and G_{yy} components over Himalaya look similar apart from their sign difference which is probably due to the fact that E–W trending structures are dominant and probably can be visualized as 2D structure. It can be easily seen that the variations of GG enhance the boundaries of the HCZ structures. The E–W GG, G_{zx} further emphasizes E–W changes in the density structures in-between the main structural trends, which may be used to model smaller near surface density variations across this terrain.

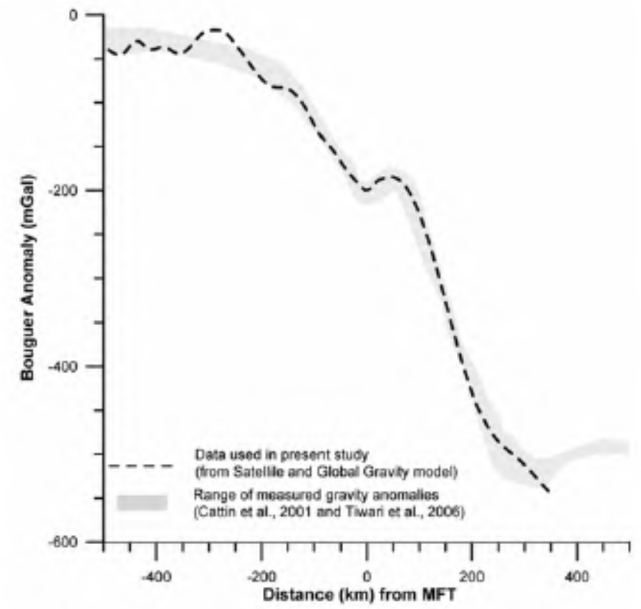

Figure 1. Bouguer anomalies projected along a profile. Shaded region shows a range of measured gravity anomalies in the Nepal, Sikkim Himalaya and Tibet[3,4]. Dashed line shows the Bouguer anomalies computed from global gravity model (EGM2008) that includes GRACE satellite gravity data and terrestrial data.

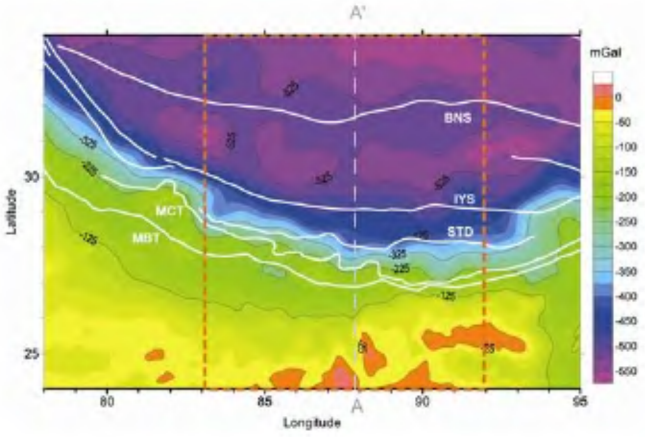

Figure 2. Bouguer gravity anomalies of the Himalaya and Tibet tectonic zone. Major tectonic boundaries; MBT: Main Boundary Thrust; MCT: Main Central Thrust, STD: Southern Tibetan detachment, IYS: Indus Yarlung Suture, BNS: Bangong-Nujiang Suture are overlaid on Bouguer Anomaly map. Rectangular area marked in red dashed line is the area of investigation. A N–S gray dashed line (A–A′) is also shown along which a lithospheric density model is shown in Figure 5.

Density model of Himalaya

A 3D density model is constructed from the Bouguer anomalies derived from global gravity models of the eastern HCZ using the IGMAS modelling software[22]. The modelling procedure is based on an interactive forward-modelling in which calculated gravity responses of the modelled geometries are compared to the observed gravity anomalies. Therefore the modelling depends on the initial geometry. The initial constraint to the geometry and densities of bodies are primarily defined from the earlier studies; seismic and seismological[23–26] gravimetry[4] and geological cross-section[27]. Geometries of the bodies are modified to best fit BGA. A vertical cross-section of the modelled lithospheric structure along a profile is plotted in Figure 5. This model shows Moho depth of about 35–37 km south of the Indo-Gangetic plane, which increases gradually towards north and later, deepens sharply near Main Central Thrust (MCT). The depth of Moho from the surface near Indus Yarlung Suture (IYS) is around 70 km. The model also suggests that Indian lower crust penetrates up to about 200 km north of IYS and lower crust north of IYS is densified. Upper crustal features are mainly related to Main boundary thrust (MBT), MCT and Southern Tibetan detachment (STD) where significant lithological changes occur (upper panel Figure 5). Five components of GG are also computed for this model to ascertain the computed GG from

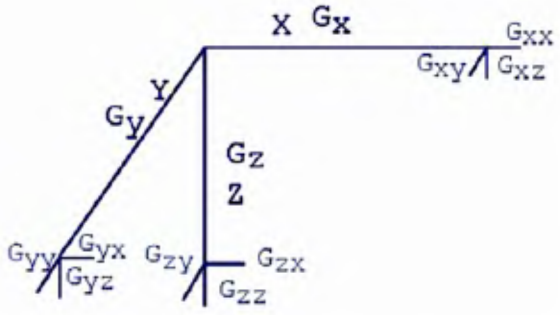

Figure 3. Schematic diagram of the gravity gradient tensors showing their directions, which are used in computation.

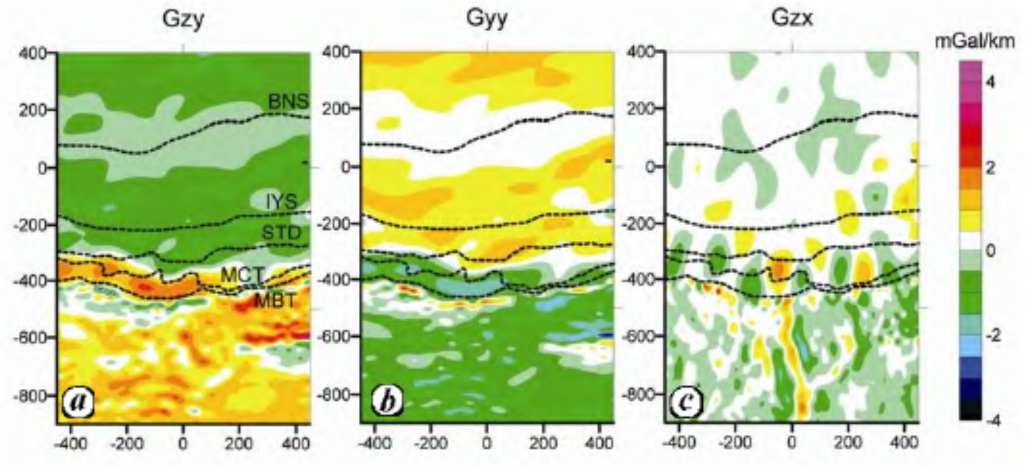

Figure 4. Three gravity gradient tensors (GG) computed from BGA are plotted. Tectonic boundaries as mentioned in Figure 2 are shown marked for visual correlation of structural features to GG. G_{zy} is multiplied by (–1) for clarity of the features.

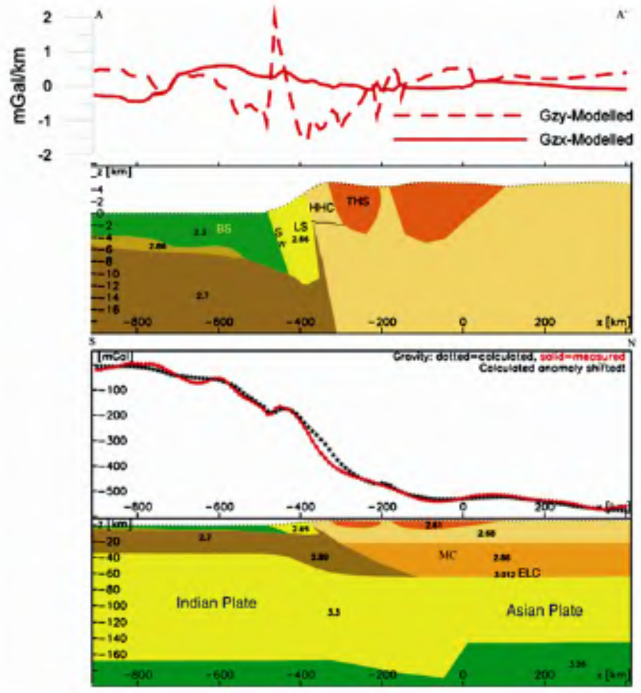

Figure 5. A vertical cross-section running from south to north of 3D density model of Eastern Himalaya computed from gravity anomalies and seismological constraints. The measured and modelled Bouguer anomalies show a good match. Computed G_{zx} and G_{zy} gradients of this model are plotted in the top panel. BS: Bengal Sediments; LC: Lesser Himalaya; HHC: Higher Himalaya Crystalline; SW: Siwalik; THS: Tethys; MC: Asian Crust; ELC: Eclogite; LC: Lower Crust. Upper panel of the figure is an exaggerated vertical cross section of upper 20 km.

BGA using Fourier transformation. Two of them are plotted in the top panel of Figure 5. The variations of G_{zx} and G_{zy} are clearly dominated by the density variations of shallow features which show the similar pattern as that computed for GG from BGA. The near surface contacts of MBT, MCT and STD are prominently reflected in these gradients rather than BGA. Model gradients from structure and computed gradients from BGA show similar nature but do not exactly match in amplitudes. For example, G_{zy} is around one in southern part, then it sharply decreases to negative values (distance – 575 km Figure 5) and again increases to positive values (distance – 475 km Figure 5); a similar trend can be seen in Figure 4 also.

Isostatic studies

Isostatic compensation of large topographic masses is a well-known phenomenon; however, there are diverse views on the mechanism of compensation. Flexural model of isostatic compensation of continental topography is now widely accepted and implies that topographic or subsurface loads are supported by the strength of the lithosphere[28]. A common proxy of lithospheric strength is the effective elastic thickness (EET), which is defined as the integrated strength of lithosphere that supports the load on geological time scale. EET is often estimated through cross spectral analyses of gravity anomalies and topography[29]. The wavelength on which transition from low coherence to high coherence commences defines EET (Figure 6). The earlier studies based on flexural modelling, thermo-mechanical modelling and spectral analyses over Himalaya suggest EET in the range of 25–60 km (refs 2–4, 6, 30). Thus the anticipated transition coherence wavelength for EET ~ 25 km (lower value of EET) will be around 200 km and therefore processed gravity anomalies over this region (BGA), which contain wavelength more than 100 km, can be utilized for the estimation of EET. There are several spectral techniques that are used for the estimation of EET[31–34]. In order to get an estimate of EET variation from these data, we used the wavelet approach[34] to compute the coherence between the gridded Bouguer anomaly and topography data. The wavelet coefficients are determined using two-dimensional Morlet wavelets[35] and theoretical coherence

is computed for a model that assumes surface and subsurface loads[29]. The estimation of error in the coherence analysis using wavelet approach is described by Swain and Kirby[35]. The estimated EET along A–A profile is plotted in Figure 7, which varies between 28 km and 48 km and estimated computational uncertainties, which is determined from fitting of modelled and computed coherence, are found in the range of 1–3 km. It is clear from Figure 7 that there are significant variations of EET across Himalaya, which have also been reported earlier[2,3]. EET decreases towards north and attains minimum value under Tibetan plateau, which can be attributed mainly due to thermal weakening though EET depends on various mechanical and thermal properties of the lithosphere together with density structure[36]. The estimates of EET from the data used in the present study are comparable to those from the studies that used terrestrial data[3,4], demonstrating applicability of global gravity models for isostatic studies.

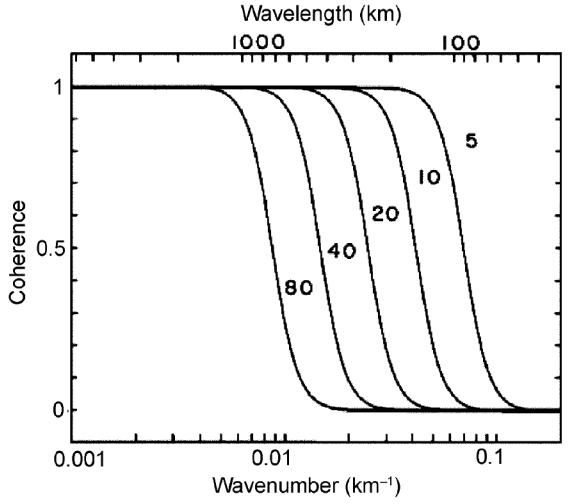

Figure 6. Theoretical coherence curves showing effective elastic thickness (EET) and wavelength at which transition of coherence from low to high commences that defines EET (after Forsyth[29]). The coherence computed for a model that assumes surface and subsurface loads.

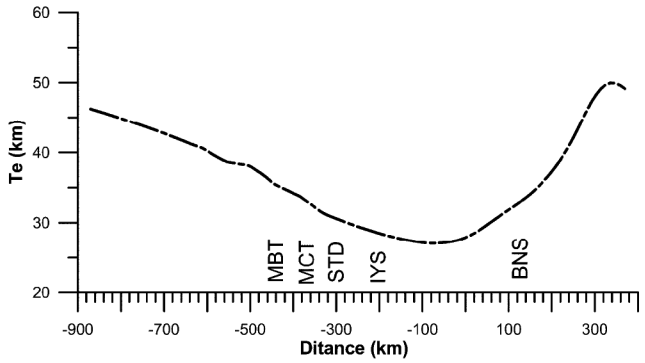

Figure 7. Estimate of effective elastic thickness (EET) plotted along a profile AA′ showing variation across Himalaya. EET decreases over collision zone and attains minima over Tibet and starts increasing after 200 km north of IZS.

Summary

In the present study attempts have been made to compute BGA from global gravity models and GG tensors from BGA to illustrate that BGA derived from global gravity models is comparable to terrestrial data for the wavelength >50 km and can be used for subsurface mapping of large structural features of HCZ, Moho depth variations and isostatic studies. This is of increasing importance as state-of-art satellite missions are able to measure minute variations of the Earth's gravity field with rapidly improving spatial accuracy. It would be of great relevance to geophysical interpretation to take advantage of this phenomenal progress in remote measurements for the detailed understanding of regional geo-tectonics, specially in inaccessible regions like the Himalaya.

A 3D density model of the Eastern Himalaya based on BGA and gradient computations from this model thereof serve to bring out the specialties of each field, suggesting the fact that a suitable combination of measured gradients and total gravity could well achieve much higher degrees of reliability of interpretation of the subsurface features. Visual comparison of the top and lower panels of Figure 5 shows that BGA bears the dominant signature of the crust–mantle boundary, whereas the nature of the gradients is dictated by the changes in the upper crustal geometry and gradients are similar to GG computed from BGA.

Similarly, inspection of BGA (Figure 2) and the gradient maps of Figure 4 indicates positive correlations of broad trends of the prominent arcuate signature of the Himalayan relief. At the same time, it is clear that gradient computations of the same gravity field do help to bring out small wavelength features associated with upper crustal features like MBT, MCT with a greater clarity. It is remarkable to note that G_{zy} and G_{yy} clearly demarcate the region between MCT and MBT, which indicates that surface expressions of tectonic features extend to the subsurface. The lateral variation along strike of HCZ, which has been noted earlier[37], can easily be brought out in the GG maps. For example G_{zx} changes between MCT and STD near zero distance longitude (Figure 4 *c*) have direct visual correlation with the changes in fractal dimensions and *b* values of earthquakes, indicating lateral variations in the crust[38]. Estimated EET provides interesting observation that the lowest value may mark the extent of Indian plate under Tibet as even suggested from seismological studies[25]. The above-mentioned examples therefore, suggest that the global gravity models particularly in the regions of insufficient data have a large potential to provide information of regional tectonics, subsurface heterogeneities, mechanical properties and so on. Availability of satellite GG data from the ongoing GOCE mission, shortly would further improve the understanding of the nature of gravity anomalies and their causative sources.

1. Valdiya, K. S., *Dynamic Himalaya*, University Press (India), Hyderabad, 1998.
2. Jin, Y., McNutt, M. K. and Zhu, Y. S., Mapping the descent of Indian and Eurasian plates beneath the Tibetan Plateau from gravity anomalies. *J. Geophys. Res.*, 1996, **101**, 11275–11290.
3. Cattin, R., Martelet, G., Henry, P., Avouac, J. P., Diament, M. and Shakya, T. R., Gravity anomalies, crustal structure and thermo-mechanical support of the Himalaya of Central Nepal. *Geophys. J. Int.*, 2001, **147**, 381–392.
4. Tiwari, V. M., Rao, M. B. S. V., Mishra, D. C. and Singh, B., Crustal structure across Sikkim, NE Himalaya from new gravity and magnetic data. *Earth Planet Sci. Lett.*, 2006, **247**, 61–69.
5. Mishra, D. C., Rajashekhar, R. P. and Ravikumar, M., Crustal structure based on satellite gravity and magnetic fields. (eds Arora, B. R. and Sharma, R.). *Mem. 72 Geol. Soc. India*, 2008, pp. 1–28.
6. Tiwari, V. M., Rajasekhar, R. P. and Mishra; D. C., Gravity anomaly, lithospheric structure and seismicity of Western Himalayan syntaxis. *J. Seismol.*, 2009; DOI:10.1007/s10950-08-9102-6.
7. Braitenberg, C. and Ebbing, J., New insights into the basement structure of the West Siberian Basin from forward and inverse modeling of GRACE satellite gravity data. *J. Geophys. Res.*, 2009, **114**, B06402; doi:10.1029/2008JB005799.
8. Fedi, M., Ferranti, L., Florio, G., Giori, I. and Italiano, F., Understanding the structural setting in the Southern Apennines (Italy): insight from gravity gradient tensor. *Tectonophysics*, 2005, **397**, 21–36.
9. Fu, L. L. and Cazenave, A., Satellite altimetry and earth sciences. In *A Handbook of Techniques and Applications*, Academic Press, 2001.
10. Reigber, Ch. *et al.*, A high quality global gravity field model from CHAMP GPS tracking data and accelerometry (EIGEN-1S). *Geophys. Res. Lett.*, 2002, **29**(14); doi:10.1029/2002GL015064.
11. Jekeli, C., The determination of gravitational potential differences from satellite-to-satellite tracking. *Celestial Mech. Dynam. Astron.*, 1999, **75**(2), 85–101.
12. Balmino, G., Gravity field recovery from GRACE: Unique aspects of the high precision inter-satellite data and analysis methods. *Space Sci. Rev.*, 2003, **108**(1–2), 47–54.
13. Tapley, B. *et al.*, GGM02 – An improved Earth gravity field model from GRACE. *J. Geod.*, 2005, **79**, 467–478.
14. Colombo, O. and Kleusberg, A., Applications of an orbiting gravity gradiometer. *Bull. Geod.*, 1983, **57**, 83–101.
15. Rummel, R. and Colombo, O., Gravity field determination from satellite gradiometry. *Bull. Geod.*, 1985, **59**, 233–246.
16. Bobojc, A. and Drozyner, A., Satellite orbit determination using satellite gravity gradiometry observations in GOCE mission perspective. *Adv. Geosci.*, 2003, **1**, 109–112.
17. Rummel, R., Satellite gradiometry. In *Lecture Notes in Earth Sciences, Mathematical and Numerical Techniques in Physical Geodesy* (ed. Sünkel, H.), Springer, Berlin, 1986, vol. 7, pp. 318–335.
18. Forste, C. *et al.*, The GeoForschungsZentrum Potsdam/Groupe de Recherche de Geodesie Spatiale satellite-only and combined gravity field models: EIGEN-GL04S1 and EIGEN-GL04C. *J. Geod.*, 2008; doi:10.1007/s00190-007-0183-8.
19. Pavlis, N. K., Holmes, S. A., Kenyon, S. C. and Factor, J. K., An earth gravitational model to degree 2160:EGM2008, Presented to EGU-2008, Vienna, Austria, April 2008.
20. GTOPO, 1997; http://edc.usgs.gov/products/elevation/gtopo30/gtopo30.html
21. Mickus, K. and Hinojosa, J. H., The complete gravity gradient tensor derived from vertical gravity data: a Fourier transform technique. *J. Appl. Geophys.*, 2001, **46**, 159–174.
22. Schmidt, S. and Gotze, H.-J., Interactive visualization and modification of 3D models using GIS functions. *Phys. Chem. Earth*, 1998, **23**(3), 289–295.
23. Hetényi, G., Cattin, R., Brunet, F., Bollinger, L., Vergne, J., Náblek, J. L. and Diament, M., Density distribution of the India plate beneath the Tibetan Plateau: geophysical and petrological constraints on the kinetics of lower-crustal eclogitization. *Earth Planet. Sci. Lett.*, 2007, **264**, 226–244.
24. Hauck, M. L., Nelson, K. D., Brown, L. D., Zhao, W. and Ross, A. R., Crustal structure of the Himalaya orogen at ~90 east longitude from INDEPTH deep reflection profiles. *Tectonics*, 1998, **17**, 481–500.
25. Kind, R. *et al.*, Seismic images of crust and upper mantle beneath Tibet: evidence for Eurasian plate subduction. *Science*, 2002, **298**, 1219–1221.
26. Schulte-Pelkum, V. *et al.*, Imaging the Indian subcontinent beneath the Himalaya. *Nature*, 2005, **435**, 1222–1225.
27. Acharya, S. K. and Ray, K. K., Geology of the Darjeeling-Sikkim Himalaya, Guide to Excursion No. 4 Fourth International Gondwana Symposium, Report 25, Calcutta, India, 1977.
28. Watts, A. B., *Isostasy and Flexure of the Lithosphere*, Cambridge University Press, 2001, pp. 1–458.
29. Forsyth, D. W., Subsurface loading and estimates of the flexural rigidity of continental lithosphere. *J. Geophys. Res.*, 1985, **90**, 12623–12632.
30. Chamoli, A., Pandey, A. K., Dimri, V. P. and Banerjee, P., Crustal configuration of the Northwest Himalaya based on modeling of gravity data. *Pure Appl. Geophys.*, 2010; doi:10.1007/s00024-010-0149-2.
31. Lowry, A. R. and Smith, R. B., Flexural rigidity of the basin and range–Colorado Plateau–Rocky mountain transition from the coherence analysis of gravity and topography. *J. Geophys. Res.*, 1994, **99**(20), 123–140.
32. Tiwari, V. M. and Mishra, D. C., Estimation of effective elastic thickness from gravity and topography data under Deccan Volcanic Province, India. *Earth Planet. Sci. Lett.*, 1999, **171**, 189–299.
33. Simons, F. J., van der Hilst, R. D. and Zuber, M. T., Spatiospectral localization of isostatic coherence anisotropy in Australia and its relation to seismic anisotropy: implication for lithospheres deformation. *J. Geophys. Res.*, 2003, **108**, 2250; doi: 10.1029/2001JB000704.
34. Kirby, J. F. and Swain, C. J., Global and local isostatic coherence from the wavelet transform. *Geophys. Res. Lett.*, 2004, **31**, doi:10.1029/2004GL02169.
35. Swain, C. J. and Kirby, J. F., The effect of 'noise' on estimates of the elastic thickness of the continental lithosphere by the coherence method. *Geophys. Res. Lett.*, 2003, **30**, 1574; doi: 10.1029/2003GL017070.
36. Burov, E. and Diament, M., The effective elastic thickness (Te) of continental lithosphere: What does it really mean? *J. Geophys. Res.*, 1995, **100**, 3905–3928.
37. Hazarika, P., Kumar, M. R., Srijayanthi, G., Raju, P. S., Rao, N. P. and Srinagesh, D., Transverse tectonics in the Sikkim Himalaya: evidence from seismicity and focal-mechanism data. *Bull. Seismol. Soc. Am.*, 2010, **100**, 1816–1822; doi: 10.1785/0120090339.
38. Singh, C., Singh, A. and Chadha, R. K., Fractal and *b*-value mapping in eastern Himalaya and southern Tibet. *Bull. Seismol. Soc. Am.*, 2009, **99**, 3529–3533; doi: 10.1785/0120090041.

ACKNOWLEDGEMENTS. We are grateful to the Director, NGRI for permission to publish this work. We also thank C. P. Rajendran, for inviting us to contribute this article. We gratefully acknowledge H.-J. Gotze and S. Schmidt for introducing us to the IGMAS software. Critical comments by Michel Diament and D. C. Mishra have improved the manuscript and we acknowledge them sincerely.